

# JGR Atmospheres

## RESEARCH ARTICLE

10.1029/2020JD033513

### Key Points:

- Our simulations suggest that the tripolar precipitation pattern in monsoonal China likely occurs on orbital timescales
- The boreal summer insolation is the dominant forcing for the intensity of East Asian summer monsoon on orbital time scales
- This study emphasizes the high complexities in hydroclimatic conditions in monsoonal China throughout the past glacial-interglacial cycles

### Supporting Information:

Supporting Information may be found in the online version of this article.

### Correspondence to:

Z. Zhang,  
[zhongshi.zhang@cug.edu.cn](mailto:zhongshi.zhang@cug.edu.cn)

### Citation:

Dai, G., Zhang, Z., Otterå, O. H., Langebroek, P. M., Yan, Q., & Zhang, R. (2021). A modeling study of the tripole pattern of East China precipitation over the past 425 ka. *Journal of Geophysical Research: Atmospheres*, 126, e2020JD033513. <https://doi.org/10.1029/2020JD033513>


Received 13 JUL 2020

Accepted 4 MAR 2021

### Author Contributions:

**Conceptualization:** Zhongshi Zhang  
**Funding acquisition:** Zhongshi Zhang  
**Investigation:** Zhongshi Zhang  
**Methodology:** Zhongshi Zhang  
**Project Administration:** Zhongshi Zhang  
**Supervision:** Zhongshi Zhang  
**Writing – original draft:** Gaowen Dai  
**Writing – review & editing:** Zhongshi Zhang, Odd Helge Otterå, Petra M. Langebroek, Qing Yan

## A Modeling Study of the Tripole Pattern of East China Precipitation Over the Past 425 ka

Gaowen Dai<sup>1</sup> , Zhongshi Zhang<sup>1,2</sup> , Odd Helge Otterå<sup>3,4</sup>, Petra M. Langebroek<sup>3</sup>, Qing Yan<sup>2</sup> , and Ran Zhang<sup>5</sup> 

<sup>1</sup>Department of Atmospheric Science, School of Environmental Studies, China University of Geosciences, Wuhan, China, <sup>2</sup>Nansen-Zhu International Research Center, Institute of Atmospheric Physics, Chinese Academy of Sciences, Beijing, China, <sup>3</sup>NORCE Norwegian Research Centre, Bjerknes Centre for Climate Research, Bergen, Norway, <sup>4</sup>Center for Early Sapiens Behaviour, Bergen, Norway, <sup>5</sup>Climate Change Research Center, Institute of Atmospheric Physics, Chinese Academy of Sciences, Beijing, China

**Abstract** The traditional paleoclimatological view suggests that monsoonal China was overall wetter when the East Asian summer monsoon (EASM) was strong. However, this view is at odds with the understanding of modern climate, which demonstrates an analogous “tripole precipitation pattern” in monsoonal China. Little is known about the spatial pattern of paleo-precipitation in monsoonal China, particularly during the past glacial-interglacial cycles. Here, we provide evidence for a potential tripole precipitation pattern in monsoonal China over the past 425 ka using climate modeling, and compare the results with paleoclimate records available from China. Our simulations illustrate that more (less) precipitation in North China and South China, and less (more) precipitation in the Central-East China during strong (weak) EASM periods associated with high (low) boreal summer insolation. Our results agree with the present understanding of modern East Asian climate, and furthermore confirm that the boreal summer insolation is the dominant forcing for the intensity of EASM and the response of subtropical high pressures is fundamental in modulating the precipitation pattern in monsoonal China on orbital timescales. This temporal and spatial variability of precipitation, as revealed in our simulations, shows the potential high complexities in hydroclimatic conditions in monsoonal China throughout the past glacial-interglacial cycles. Nevertheless, whether the tripole precipitation pattern in monsoonal China over the past 425 ka is robust enough still should be tested, preferable by taking advantage of existing and new well-dated and explicit indicative precipitation archives in Central-East China.

## 1. Introduction

In paleoclimate studies, it is widely believed that monsoonal China receives more precipitation when the East Asian summer monsoon (EASM) is stronger (e.g., Zhou, Xian, et al., 2014). However, many studies of modern climate show some conflicts with this widely held concept in paleoclimate studies. Modern climate observations often show a tripolar precipitation pattern in monsoonal China during the past several decades (e.g., Ding et al., 2008). When the EASM is strong (weak), more (less) precipitation falls over the Yellow River Valley (North China, NC) and the Pearl River Valley (South China, SC) while less (more) precipitation appears in the Yangtze River Valley (Central-East China, CEC) (Figure S1). This analogous tripolar precipitation pattern in monsoonal China is also observed since the Last Glacial Maximum (Chen et al., 2015; E. Huang et al., 2018; X. Huang et al., 2018; Jia et al., 2015; W. Jiang et al., 2006; Jin et al., 2014; H. Liu et al., 2019; Lu et al., 2019; S. Wang et al., 2007; Xiao et al., 2004; Xie et al., 2013; H. Zhang et al., 2018; Zhou, Yu, et al., 2004; Zhu et al., 2017).

However, little is known about changes in the spatial patterns of precipitation in monsoonal China before the Last Glacial Maximum, during the past glacial-interglacial cycles. Most paleo-precipitation records on the orbital timescale are found in the Chinese Loess Plateau in NC (Beck et al., 2018; Li et al., 2017; Ning et al., 2008; Peterse et al., 2014; Sun et al., 2015; Thomas, Clemens, Sun, et al., 2016; Z. Wang et al., 2018; Zhou, Xian, et al., 2014) and the South China Sea (e.g., E. Huang et al., 2018; Thomas, Clemens, Prell, et al., 2014). These records show consistent variations in precipitation, which tend to follow the boreal summer insolation closely (Figures 1a and 1d). However, the proxies from Tai Lake (Miao et al., 2015) and Weinan (Thomas, Clemens, Sun, et al., 2016) in (or close to) the CEC show opposite changes. Relatively wet

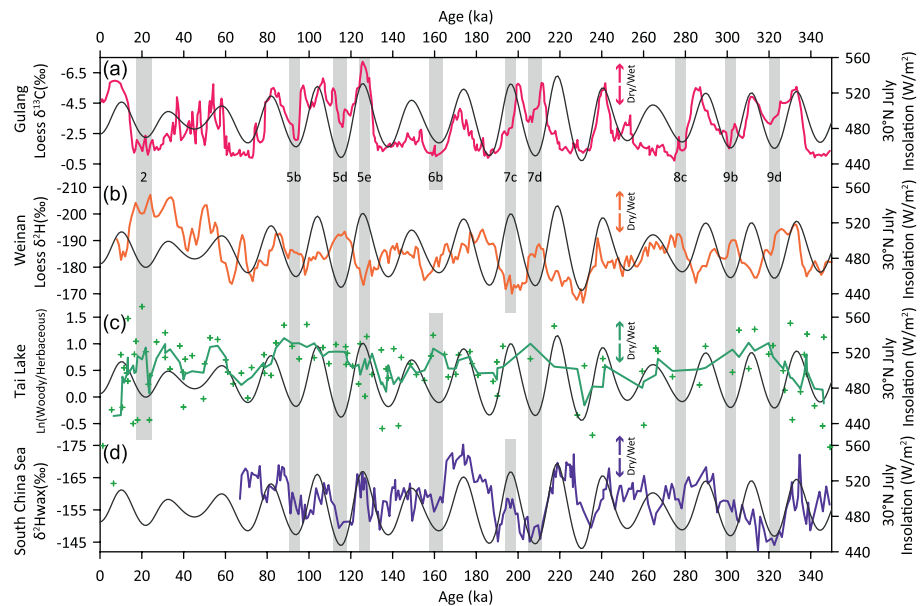


**Figure 1.** Potential dry and wet climate state reflected by geological records. (a) Loess  $\delta^{13}\text{C}$  from Gulang (37.48°N, 102.87°E, North China; Sun et al., 2015). (b) Loess  $\delta^2\text{H}_{\text{wax}}$  from Weinan (34.42°N, 109.6°E, south margin of Chinese Loess Plateau, near Central-East China; Thomas, Clemens, Sun, et al., 2016). (c) The pollen ratio of Woody/Herbaceous from Tai Lake (31.5°N, 120.45°E, Central-East China; Miao et al., 2015), the green curve is the result of original pollen ratios (green crosses) by three-point moving average. (d) The marine sediment biomarker records  $\delta^2\text{H}_{\text{wax}}$  from ODP Site 1146 (19.45°N, 116.27°E, South China; Thomas, Clemens, Prell, et al., 2014). The black curves represent 30°N July insolation (Laskar et al., 2004), and gray bars indicate the stages of resembling tripolar precipitation pattern. Here, for (a, b, and d), the chronologies are based on the radiometrically calibrated age model, the control point ages are mainly from comparison between the mean grain size of loess or benthic  $\delta^{18}\text{O}$  of marine sediments and the standard benthic  $\delta^{18}\text{O}$  (Lisiecki & Raymo, 2005) or well dated speleothem records; for (c), the chronologies are obtained by the linear interpolation between the  $^{14}\text{C}$  age and B/M boundary (780 ka).

conditions occur several times, typically coinciding with low boreal summer insolation (Figures 1b and 1c). Although many stalagmites oxygen isotope records ( $\delta^{18}\text{O}$ ) have been reported from the Yangtze River Valley, controversial interpretations of stalagmite  $\delta^{18}\text{O}$  bring uncertainties in interpreting variations in regional precipitation amount (e.g., Cheng, Zhang, et al., 2019).

Although a few precipitation reconstructions suggest opposite variations in precipitation amount in CEC relative to in NC and SC, whether the tripolar precipitation pattern in monsoonal China appears on orbital timescales remains an unresolved question. To address this question, in this study we use the low-resolution version of the Norwegian Earth System Model (NorESM-L) to simulate the East Asian climate change over the past 425 ka. In this paper, we first describe the model and experimental design in Section 2. Section 3 shows our results and related mechanism. Section 4 shows our discussions and summaries.

## 2. Method

### 2.1. Model Introduction

The Norwegian Earth System Model (NorESM) is a fully coupled Earth System Model (Bentsen et al., 2013), which is developed from the Community Earth System Model (CESM; see the CESM website at <http://www2.cesm.ucar.edu/>). It is structured by the same atmosphere (CAM4), land (CLM4), sea ice (CICE4), and coupler (CLP7) components as the CESM, but with a different ocean component. The low-resolution version NorESM-L is developed for paleoclimate simulations (e.g., Zhang, Nisancioglu, et al., 2012; Zhang, Ramstein, et al., 2014). The NorESM-L couples the Miami Isopycnic Coordinate Ocean Model (MICOM) and the spectral Community Atmosphere Model (CAM4) (Eaton, 2010; Neale et al., 2013). The horizontal resolution of the MICOM is nearly  $3^\circ$  (g37), and 32 layers in the vertical. The horizontal resolution of the

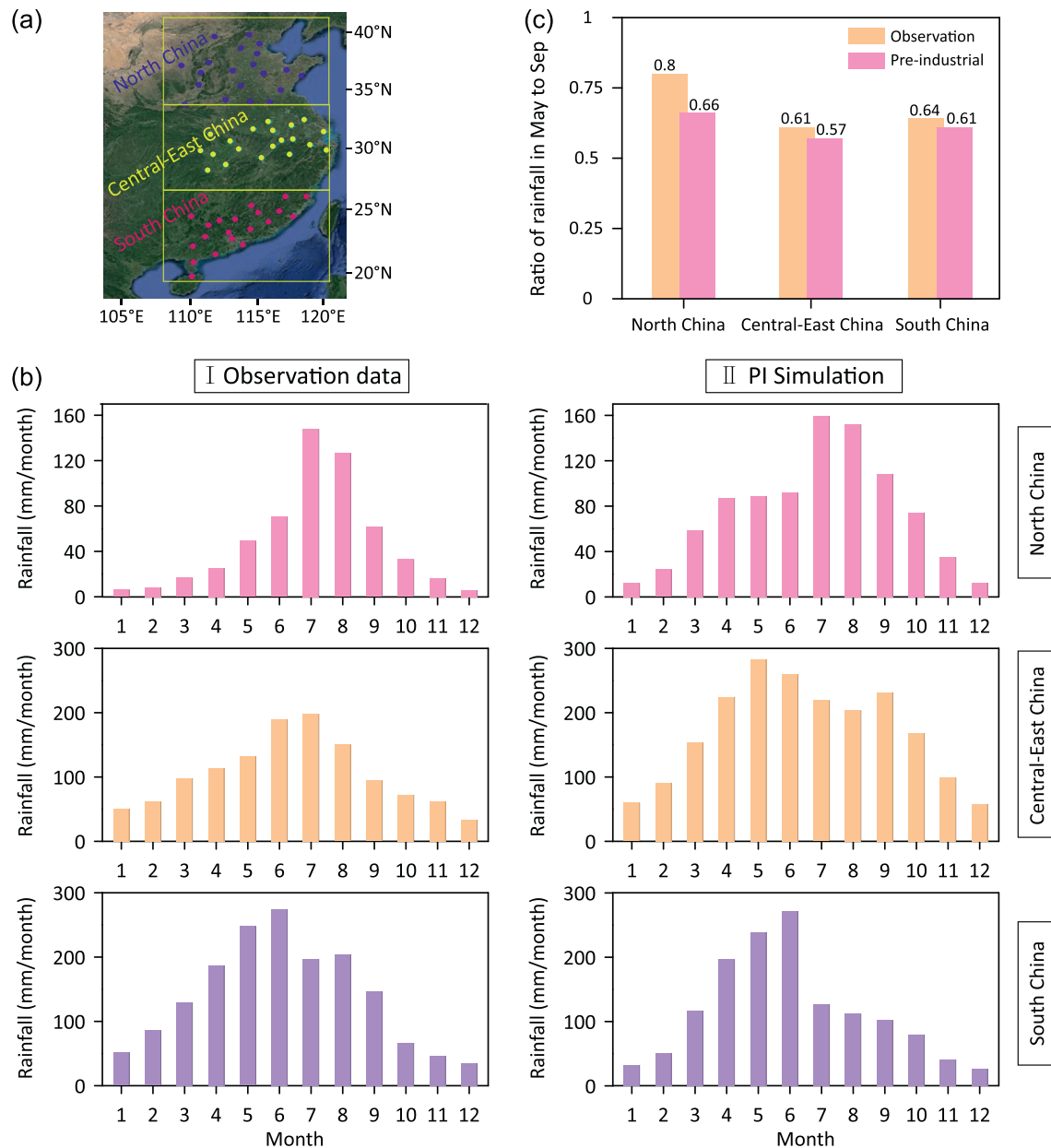


**Figure 2.** (a) The location of the 60 meteorological stations in East China. The blue, yellow, and red dots, respectively indicate meteorological stations in North China, Central-East China and South China. (b) Comparison of the monthly precipitation in North China, Central-East China, and South China. (c) The precipitation in monsoon rainy season (from May to September) accounts for the proportion of the whole year. The observation rainfall data for 1981–2010 can be downloaded from the website (<http://data.cma.cn/data/weatherBk.html>).

CAM4 is about  $3.75^\circ$  (T31), with 26 layers in the vertical. The detailed introduction of NorESM-L can be found in Zhang, Nisancioglu, et al. (2012) and Bentsen et al. (2013).

The atmosphere module CAM4 includes physical parameterizations of convection, clouds, surface processes, and turbulent mixing. Its deep convection parameterization has been improved compared to the earlier versions, which have increased the convection sensitivity to tropospheric moisture and reduced the amplitude of the diurnal cycle of precipitation over land (Neale et al., 2013). The CAM4 simulates the precipitation in East Asia realistically (R. Zhang et al., 2017). In the pre-industrial (PI) experiment (see Section 2.2), it overall displays a monthly precipitation distribution similar to observations (Figure 2b), in which the monsoon precipitation in the rainy season (from May to September) accounts a major proportion of the whole

year (Figure 2c). Although some discrepancies exist between the simulated and observed absolute precipitation value (Figure 2b), these discrepancies will be reduced by calculating anomalies in the precipitation.

## 2.2. Experimental Design

Based on relative maxima, minima and median points of July insolation at 65°N (Berger & Loutre, 1991), we run 77 equilibrium simulations to capture climate variation during the past 425 ka. These experiments are forced by orbital parameters (Berger, 1978), greenhouse gas (CO<sub>2</sub> (Luthi et al., 2008), CH<sub>4</sub> (Loulergue et al., 2008) and simulated (Zhang, Yan, et al., 2020) or reconstructed (Peltier et al., 2015) Northern Hemisphere (NH) ice sheets at the selected time slices. The simulated NH ice sheets have been introduced in an experimental flow as described in Zhang, Yan, et al. (2020). The ICE6G reconstructed ice sheets are also implemented in the simulations during the last glacial-interglacial cycle (Peltier et al., 2015). In our simulations, the vegetation cover in East Asia remains the same as in the PI experiment. The details of the experimental set-up can be found in Zhang, Yan, et al. (2020). In addition, PI and mid-Holocene (6 ka) simulations are also conducted according to the standardized experimental design from the Paleoclimate Modeling Intercomparison Project Phase 3 (PMIP3) (see the PMIP 3 website at <https://pmip3.lscce.ipsl.fr/>).

## 3. Results

### 3.1. Tripolar Precipitation Pattern Since the Last Glacial Maximum

To first validate our model, we compared our simulated climate with relevant geological evidence from monsoonal China (Figure 3) in the mid-Holocene (6 ka) and the Last Glacial Maximum (~22 ka). Although the resolution of the component in NorESM-L is coarse, it realistically simulates the 6 ka and 22 ka paleoclimates, which agree well with previous simulations in PMIP and precipitation reconstructions. Our simulations and early precipitation reconstructions (Chen et al., 2015; E. Huang et al., 2018; X. Huang et al., 2018; Jia et al., 2015; W. Jiang et al., 2006; H. Liu et al., 2019; Lu et al., 2019; Miao et al., 2015; Thomas, Clemens, Sun, et al., 2016; S. Wang et al., 2007; Xiao et al., 2004; Xie et al., 2013; H. Zhang et al., 2018; Zhou, Yu, et al., 2004; Zhu et al., 2017) show the tripolar precipitation pattern in monsoonal China.

In a good agreement with earlier PMIP simulations (Jiang, Tian, & Lang, 2013), our mid-Holocene simulation shows that the precipitation decreases in CEC, but increases in NC and SC during the mid-Holocene period, when the summer monsoon is intensified compared to the PI (Figures 3a and 3b). This tripole precipitation pattern in monsoonal China was also illustrated in the ensemble mean of mid-Holocene simulations in PMIP (Jiang, Tian, & Lang, 2013). The simulated tripole precipitation pattern agrees well with recent paleo-precipitation reconstruction in monsoonal China (Figures 3a and 3b). For example, during mid-Holocene, the lake sediments (e.g., Chen et al., 2015; Jia et al., 2015) illustrate a relatively wetter condition in both NC and SC, while the biomarker records derived from the peatland in the Yangtze River Valley (e.g., E. Huang et al., 2018; X. Huang et al., 2018; Xie et al., 2013) document a relative drier climate in CEC (Figures 3a and 3b).

Consistent with earlier PMIP simulations (Jiang, Lang, et al., 2011), our 22 ka simulation shows that the precipitation decreases in monsoonal China compared to the PI (Figure S2). However, when we compare the simulations of 22 ka and 10 ka, the tripolar precipitation pattern appears again (Figures 3c and 3d). When the summer insolation is increased from 22 ka to 10 ka, the simulated precipitation increases in NC and SC, but decreases in CEC. These simulated changes in precipitation agree well with geological reconstructions. In CEC, in addition to the records from Weinan (Thomas, Clemens, Sun, et al., 2016) and Tai Lake (Miao et al., 2015), and the recent published paleo-hydrological record from the Yangtze River Valley (H. Zhang et al., 2018), show relative drier condition during the period of early Holocene (10 ka) compared with the Last Glacial Maximum (~22 ka) (Figures 3c and 3d).

### 3.2. Modeling the Distribution of Monsoonal China Precipitation

During the past four glacial-interglacial cycles, the simulated East Asian summer monsoon intensity (EASMI) fluctuated following the variation of boreal summer insolation. All the three EASM indices (based on  $U_{850}$  (B. Wang et al., 2008),  $V_{850}$  (revised by Y. Wang et al. [2001]) and sea level pressure (SLP; Zhu &



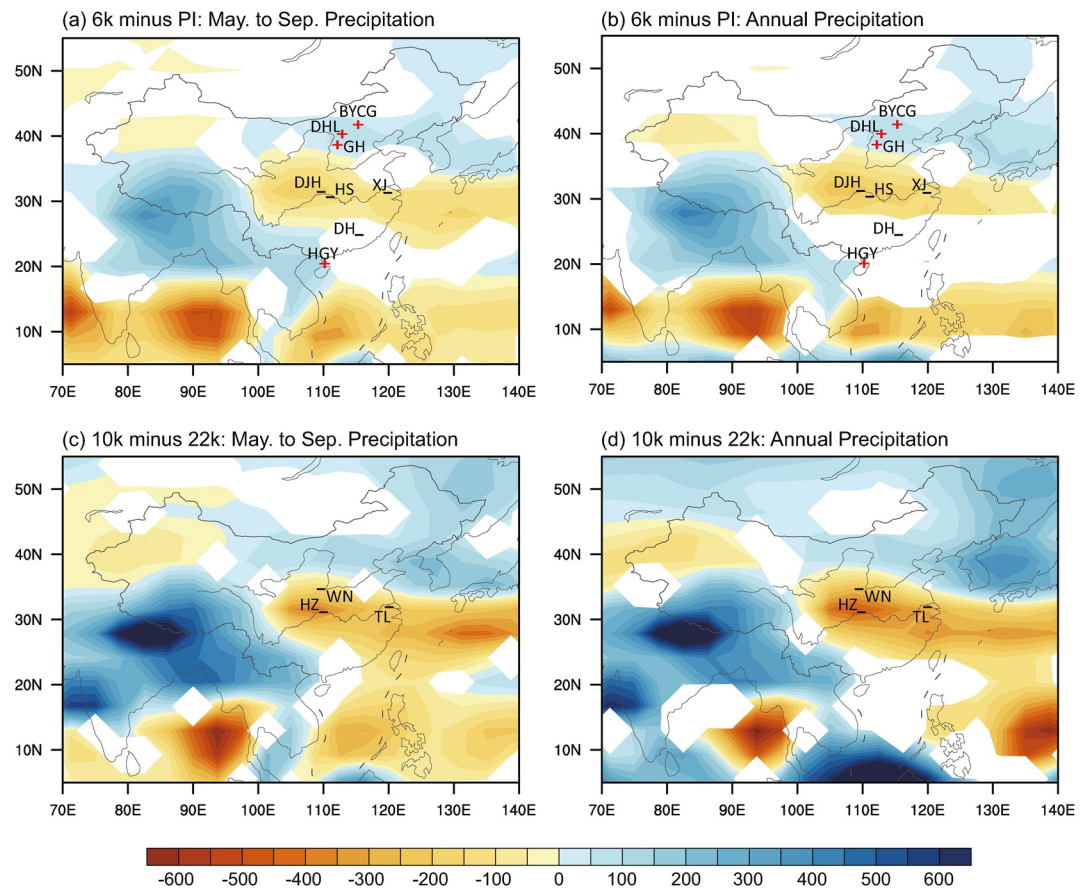


**Figure 3.** Simulated tripole pattern precipitation in monsoonal China corresponding to geological records since Last Glacial Maximum (~22 ka). (a and b) Mid-Holocene (6 ka) minus PI (unit: mm). (c and d) 10 ka minus 22 ka (unit: mm). Here, in this figures, 10 ka and 22 ka experiments forced with ICE6G reconstructed ice sheets are used. Only changes that are significant at the 95% confidence level are shown. Here, the red crosses show the relative wetter conditions and black bars show the relative drier conditions from geological evidence. Within (a and b), BYCG (Bayanchagan Lake; W. Jiang et al., 2006), DHL (Daihai Lake; Xiao et al., 2004); GH (Gonghai Lake; Chen et al., 2015) locate in North China; and HGY (Huguangyan Maar Lake; Jia et al., 2015; S. Wang et al., 2007) locates in South China; DJH (Dajiuhu; E. Huang et al., 2018; X. Huang et al., 2018; H. Liu et al., 2019; Xie et al., 2013), HS (Heshang Cave; Zhu et al., 2017), XJ (Xinjie Site; Lu et al., 2019) and DH (Dahu; Zhou, Yu, et al., 2004) are in Central-East China. Within (c and d), HZ (Haozhu Cave; H. Zhang et al., 2018), TL (Tai Lake; Miao et al., 2015) and WN (Weinan; Thomas, Clemens, Sun, et al., 2016) locate in (near) Central-East China.

Wang, 2001)) show that the simulated EASMI follows the boreal summer insolation closely (Figures 4c–4e). When the boreal summer insolation is high (low), the EASMI is strong (weak). The correlation coefficient between the simulated three EASMI (or ICE6G) and the July insolation at 30°N is 0.49, 0.72, and 0.70 (or 0.50, 0.62, and 0.76 for ICE6G) (Figures 5a–5c and 6a–6c). Moreover, our simulated EASMI (or ICE6G) corresponds well with the stalagmite  $\delta^{18}\text{O}$  record from the Sanbao cave in CEC (Figures 4b–4e; Cheng, Edwards, et al., 2016) and presents a relatively high correlation with the Sanbao cave  $\delta^{18}\text{O}$  record ( $r^2 \geq 0.3$ ; Figure S3), except one low correlation coefficient (0.19) between the EASMI<sub>V850</sub> and stalagmite  $\delta^{18}\text{O}$  (Figure S3b).

The simulated tripolar pattern is evident in the precipitation field in monsoonal China on the orbital timescale. In particular, the simulated variations of monsoon precipitation in the rainy season (from May to September) and the annual precipitation in CEC are opposite to those in NC and SC, and inversely correlated with fluctuations of EASMI (Figures 4f–4k). During the past 425 ka, there are 20 transitions in boreal summer insolation from minima to maxima (Table S1). For these 20 transitions, more than 15 show that the increased summer insolation enhanced EASMI, which increases rainy season (from May to September)

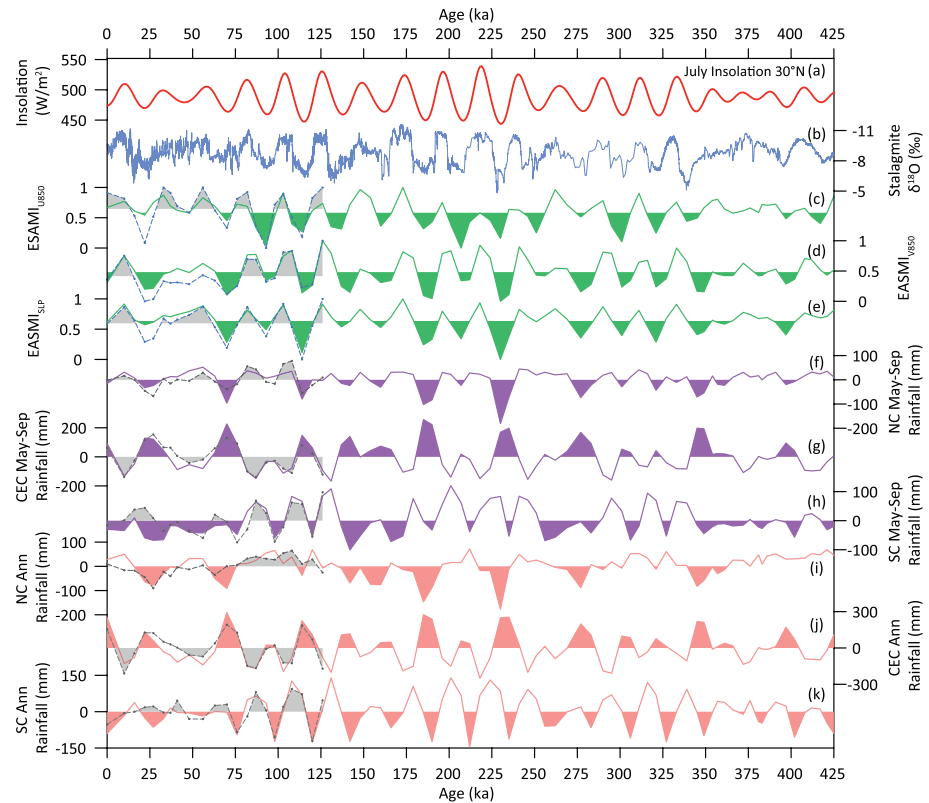


**Figure 4.** Time series of simulated East Asian summer monsoon intensity (EASMI) and corresponding precipitation anomaly in monsoonal China. (a) July insolation at 30°N (Laskar et al., 2004). (b) Speleothem  $\delta^{18}\text{O}$  from Sanbao Cave (31°40'N, 110°26'E, central China; Cheng, Edwards, et al., 2016). (c–e) respectively show the simulated EASMI calculated by zonal wind at 850 hPa (B. Wang et al., 2008), meridional wind at 850 hPa (revised from Y. Wang et al. [2001]) and sea level pressure (Zhu & Wang, 2001). All the indices are normalized. (f–h) May to September precipitation anomaly in North China (34°N–42°N, 108°E–122°E), Central-East China (26°N–34°N, 108°E–120°E), South China (18°N–26°N, 108°E–120°E), respectively. (i–k) show annual mean precipitation anomaly in North China, Central-East China, and South China, respectively. For (f–k), dashed lines are for ICE6G results over the past 126 ka.

precipitation and annual precipitation in the main part of NC and some parts of SC, while at the same time decreasing precipitation in CEC (Figure 7; Figures S4 and S5).

The simulated tripolar precipitation pattern in monsoonal China agrees with the long time series of geological evidence available from China to some extent. Over lower reaches of the Yangtze River Valley (Tai Lake Basin, CEC), as well as the region close to CEC (Weinan, south of the Chinese Loess Plateau), the moisture conditions as suggested by pollen (Miao et al., 2015) and leaf wax  $\delta^2\text{H}$  (Thomas, Clemens, Sun, et al., 2016) records show some antiphase relationship with the boreal summer insolation (Figures 1b and 1c). For example, during the MIS (Marine Isotopic Stages) 2, 5b, 5d, 6b, 7d, 8c, 9b, and 9d, when the boreal summer insolation is low, wetter conditions (the higher ratio of wood plants and herbaceous plants or more negative value of  $\delta^2\text{H}_{\text{wax}}$ ) occur in (or close to) the CEC (Miao et al., 2015; Thomas, Clemens, Sun, et al., 2016), while less precipitation (more positive value of  $\delta^{13}\text{C}$  and  $\delta^2\text{H}_{\text{wax}}$ ) appears both in NC and SC (Sun et al., 2015; Thomas, Clemens, Prell, et al., 2014; Figure 1).

### 3.3. Mechanism for the Simulated Tripole Pattern in Precipitation

Our simulations demonstrate that orbital forcing is the first-order forcing for the variations in monsoon intensity in East Asia (Figures 5 and 6), consistent with previous studies (e.g., Shi et al., 2011). The changes in boreal summer insolation modify the land-sea thermal contrasts in East Asia. The increase in boreal summer insolation warms the Asian continent more than the surrounding ocean (Figure 8a). As a result,

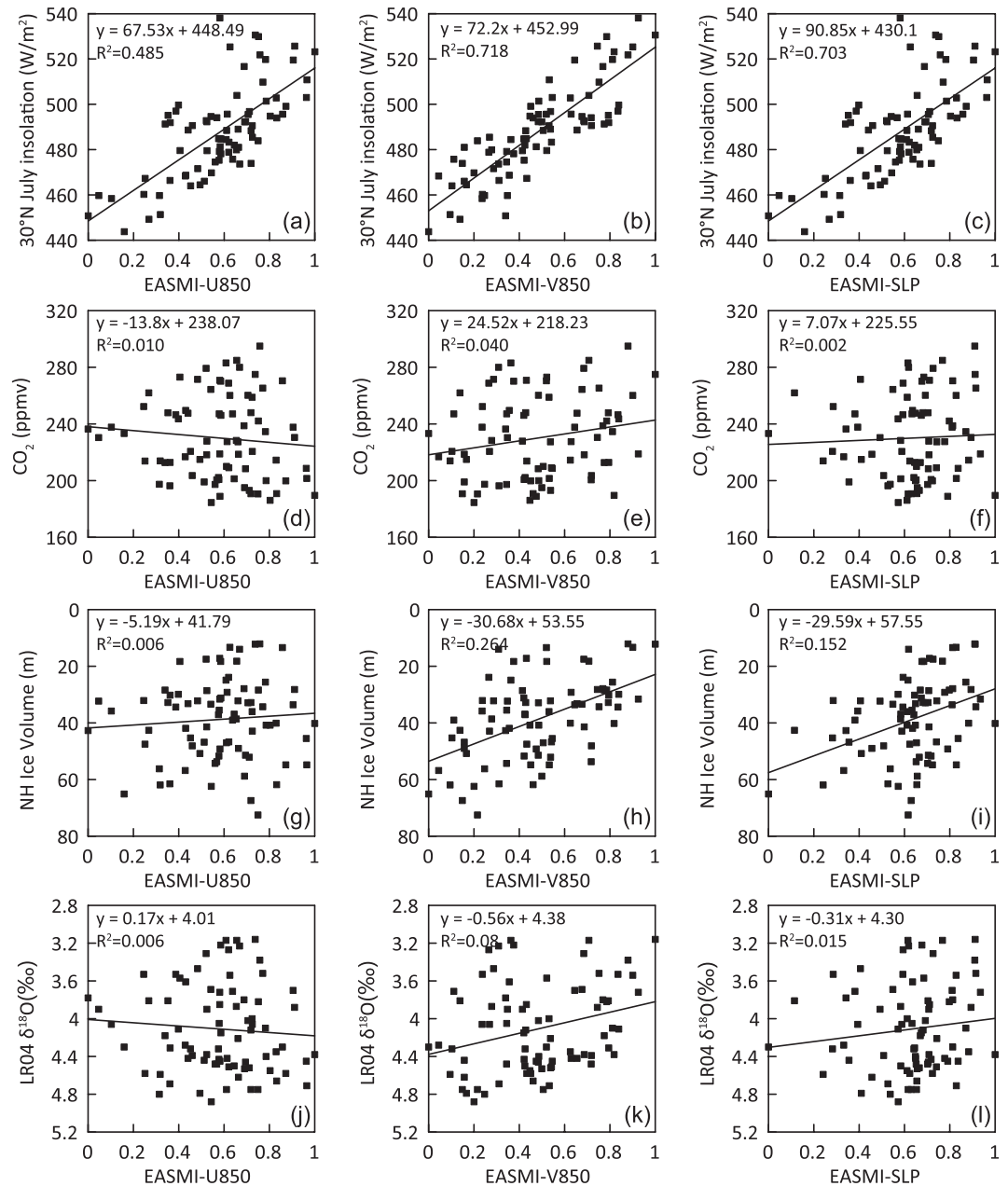


**Figure 5.** Correlation analysis between the simulated EASMI and external forcing factors. (a–c) are for insolation (Laskar et al., 2004); (d–f) are for atmospheric CO<sub>2</sub> levels (Luthi et al., 2008); (g–i) are for simulated Northern Hemisphere ice volume (Zhang, Yan, et al., 2020); and (j–l) are for global ice sheet (LR04, Lisiecki & Raymo, 2005). All the correlation analyses are on the same time scale.

the sea level pressure is further decreased over the Asian continent in summer (Figure S6a), favoring the intensification of EASM and moisture transport into monsoonal China (Figure 7).

Although the increased boreal summer insolation makes the EASM intensified, as well as the moisture transport, it also strengthens and widens the Hadley circulation, making the sinking branch of Hadley circulation moved northward (Figures 8b and S6b; X. Liu et al., 2017). As a result, the enhanced subtropical high pressures (including the western Pacific subtropical high) control the regions further north, in the insolation maxima scenarios (Figure 8c), when compared to the insolation minima scenarios (Figure 8d). Meanwhile the westerly jet becomes weaker and retreats northward (Figures 8c and 8d). These

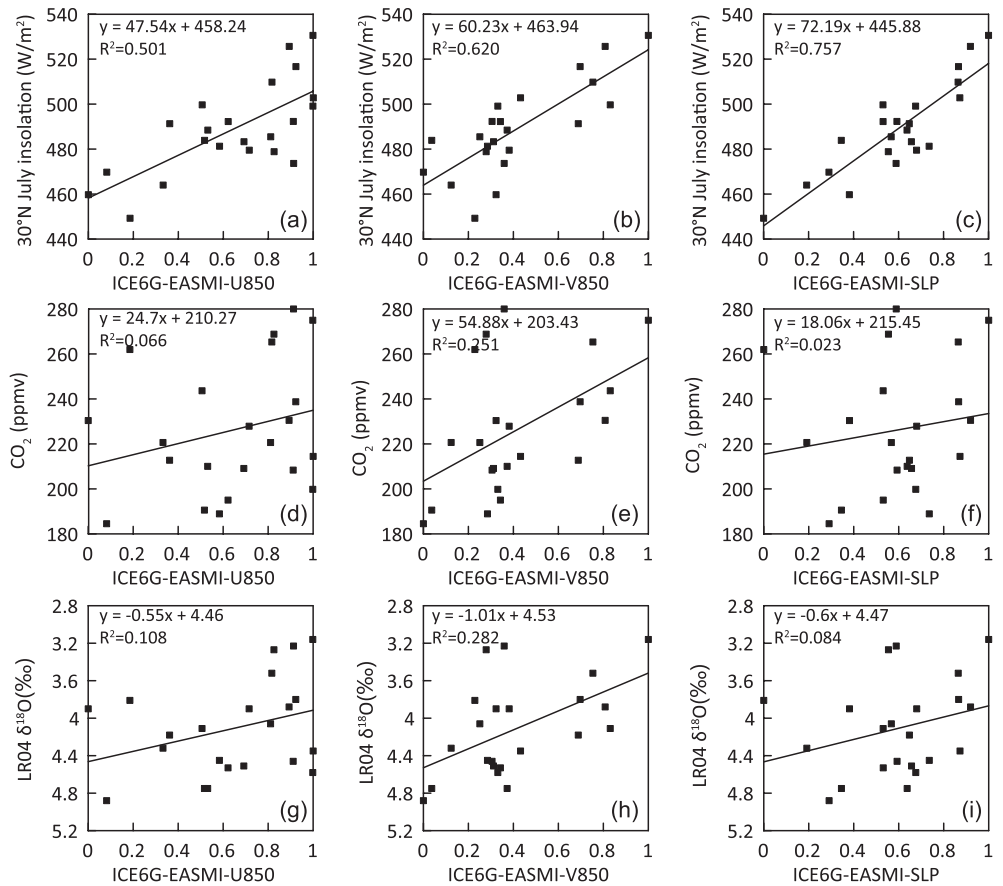


**Figure 6.** Correlation between simulated EASMI based on ICE6G experiments and external forcing factors (refer to Figure 5). Here, (a–c) are for insolation (Laskar et al., 2004); (d–f) are for atmospheric CO<sub>2</sub> levels (Luthi et al., 2008); and (g–i) are for global ice sheet (LR04, Lisiecki & Raymo, 2005). All the correlation analyses are on the same time scale.

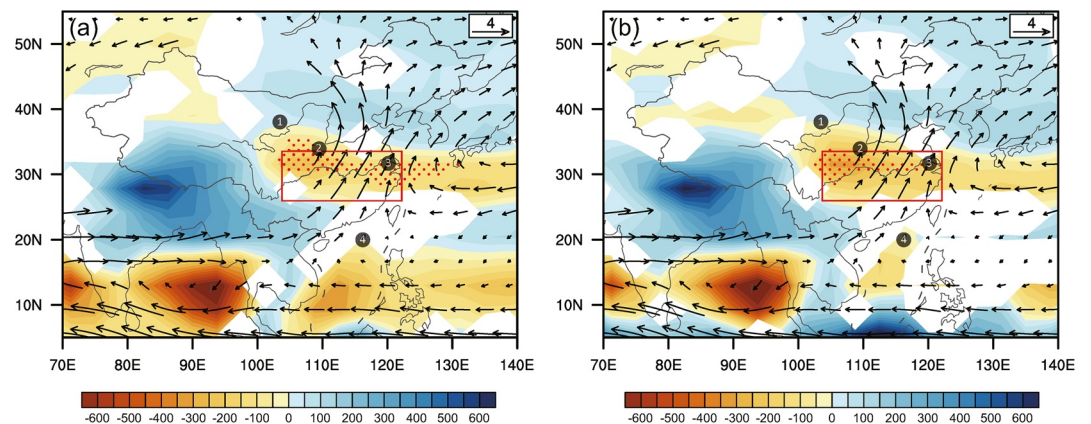


**Figure 7.** The changes in ensemble mean precipitation (unit: mm, shading colors) due to intensified summer monsoon (20 insolation maxima minus 20 insolation minima). (a) Precipitation anomalies from May to September. (b) Anomalies in annual mean precipitation. Only changes that are significant at the 95% confidence level are shown. For both (a and b), the black vectors indicate the anomaly summer (JJA) wind (m/s) at 850 hPa due to intensified summer monsoon. The red dots indicate the region where the numbers of decreased precipitation are over 15 in all the 20 samples (marked in Table S1) in monsoonal China. The numbers 1, 2, 3, and 4 indicate the location of the Gulang, Weinan, Tai Lake, and ODP Site 1146, respectively. The red rectangle shows the Central-East China region.



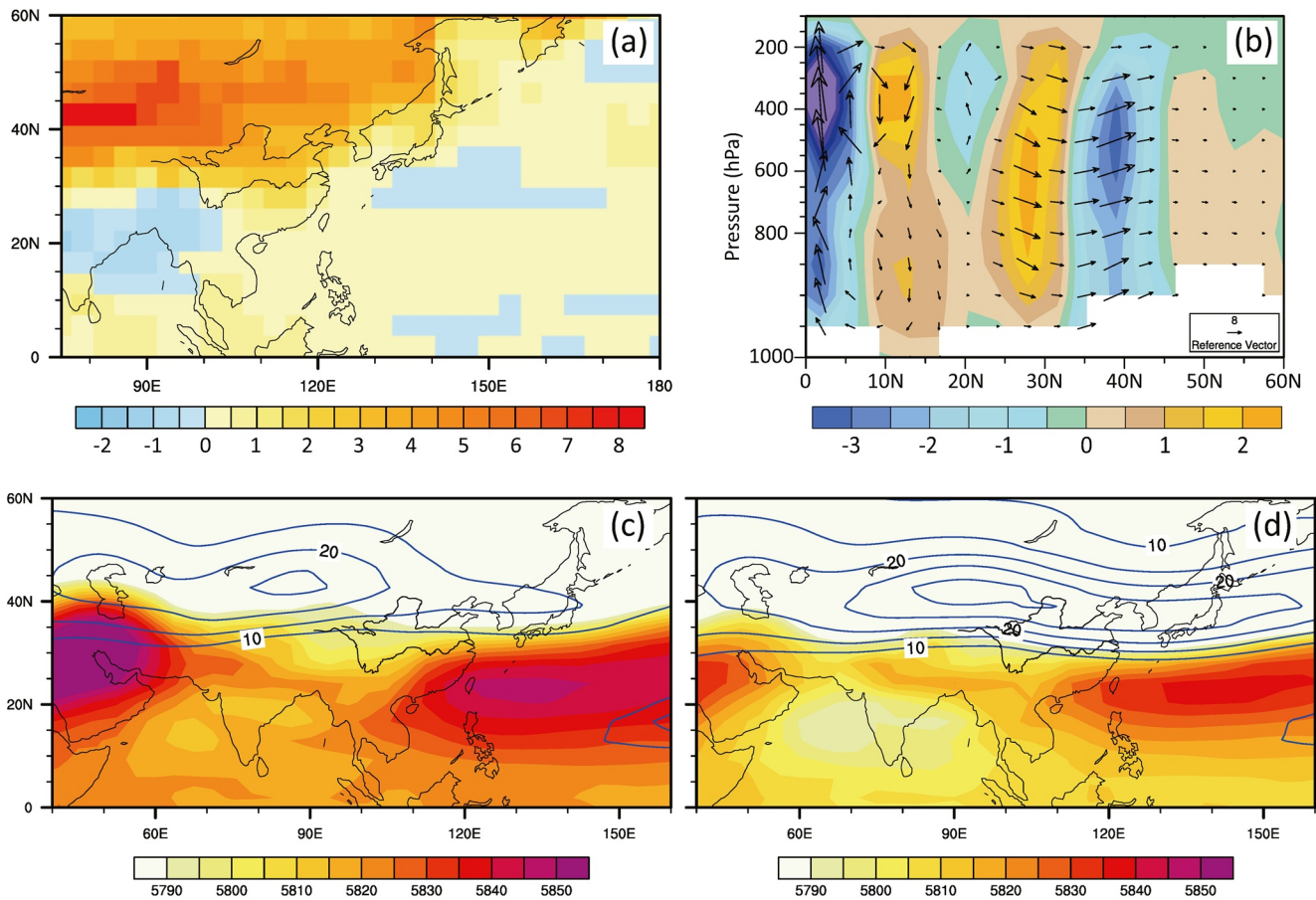


**Figure 8.** The simulated ensemble mean climatic anomaly due to intensified summer monsoon (20 insolation maxima minus 20 insolation minima). (a) The anomaly summer (JJA) surface temperature ( $^{\circ}\text{C}$ ). (b) The shading colors show the  $115^{\circ}\text{E}$  anomaly summer (JJA) vertical movement ( $\Omega$ , which is magnified by one hundred times, unit:  $\text{Pa/s}$ ; and the positive value indicates enhanced descending motion); the vector arrows indicate the  $115^{\circ}\text{E}$  anomaly JJA meridional wind ( $V$ , unit:  $\text{m/s}$ ) and vertical movement ( $\Omega$ , magnified by 700, unit:  $\text{Pa/s}$ ). For (c and d), blue contour lines show the summer (JJA) zonal wind ( $U$ , unit:  $\text{m/s}$ ,  $\geq 10 \text{ m/s}$  displayed) at 200 hPa, indicating the westerly jet; the shading colors show the summer (JJA) geopotential height (unit:  $\text{gpm}$ ) at 500 hPa, indicating the western Pacific subtropical high. Here, (c) is for the maximal insolation periods and (d) is for the minimal insolation periods.

responses simulated in our studies are in a good agreement with earlier PMIP simulations (e.g., Jiang, Tian, & Lang, 2013; Kong et al., 2017). Furthermore, the remote upstream and downstream responses due to the increased diabatic heating over continents (Rodwell & Hoskins, 2001), as well as the modest sea surface temperature decrease over the subtropical Pacific caused by ocean feedbacks (Liu, Harrison, et al., 2004), also contribute to the westward extension of the western Pacific subtropical high. This makes the western Pacific subtropical high enhanced and extends relatively northward. In this way, the intensified subtropical high pressures limit summer precipitation in CEC (Figures 8b and 8c; Kuang & Zhang, 2006; Liu, Harrison, et al., 2004; Zhou & Yu, 2005), when the NH receives more radiant energy in summer, though the EASM is stronger at this time. Thus, the precipitation variation in CEC is the key in regulating the tripolar precipitation pattern in monsoonal China on the orbital time scales. It should be noticed that this mechanism on the orbital time scales must be distinguished from the mechanism for the tripole precipitation pattern on the decadal time scales. On the decadal time scales, the westward migration of western Pacific subtropical high is caused by a regional anomalous heating forcing, for example in the Indian Ocean (T. Zhou et al., 2009), not accompanied with the intensification of whole subtropical high pressures.

## 4. Discussion and Summary

### 4.1. Insolation Forcing for Simulated Tripole Precipitation Pattern

Our simulations suggest that the boreal summer insolation is the dominating forcing for explaining variations in the intensity of EASM and simulated tripolar precipitation pattern in monsoonal China on orbital time scales. Other factors such as atmospheric greenhouse gas levels, ice sheet configurations and vegetation conditions, seem less important. In general, the EASM is strong when the atmospheric greenhouse gas levels are high. However, in the past four glacial-interglacial cycles, our simulations show several time periods (for example, at 103 and 114 ka) that produce higher EASMI, but with low greenhouse gas concentrations (Figure S7). The correlation coefficient between the simulated EASMI (or ICE6G-EASMI) and atmospheric CO<sub>2</sub> levels is less than 0.04 (less than 0.25, or even negative) (Figures 5d–5f and 6d–6f), which is much lower than the correlation coefficient (~0.49–0.73) between the EASMI (or ICE6G-EASMI) and boreal summer insolation (Figures 5a–5c and 6a–6c). Moreover, the correlation coefficient between the simulated EASMI and the NH ice volume are low (less than 0.26; Figures 5g–5i; Zhang, Yan, et al., 2020). Such a weak correlation also appears in the simulated EASMI (or ICE6G-EASMI) and LR04  $\delta^{18}\text{O}$  from Lisiecki and Raymo (2005) (Figures 5j–5l and 6g–6i). Finally, we did not include dynamic East Asian vegetation changes in our model, but stipulate that enhanced summer insolation will expand vegetation in East Asia (Yin & Berger, 2012), which may further amplify the tripolar precipitation pattern in the monsoonal region.

### 4.2. Model-Data Discussion

Although an increasing number of geological records show that CEC is relatively drier during some periods when summer insolation is higher and East Asian monsoon is stronger (X. Huang et al., 2018; H. Liu et al., 2019; Lu et al., 2019; Xie et al., 2013; H. Zhang et al., 2018; Zhu et al., 2017), for example, mid-Holocene (6 ka) versus PI, and 10 versus 22 ka (Figure 3), only a few long records currently available can confirm the existence of this negative relationship during the past 425 ka. There are two records that can be used to indicate precipitation over the past 425 ka. One is the leaf wax  $\delta^2\text{H}$  records from Weinan located in the north margin of CEC (Thomas, Clemens, Sun, et al., 2016), the other is the pollen records from Tai Lake located in the mid-east of CEC (Miao et al., 2015). These two records show relatively wetter conditions in CEC during some weak summer monsoon stages, when NC and SC are relatively dry (Sun et al., 2015; Thomas, Clemens, Prell, et al., 2014; Figure 1). However, the negative correlation between the records from (or close to) CEC and the summer insolation is not significant. The correlation coefficient is less than 0.02. This insignificant correlation could partly be due to the uncertainties in age controls and interpretations of these records. To some extent, the pollen and loess leaf wax  $\delta^2\text{H}$  proxies could also reflect the mixed signal of both precipitation and temperature. Therefore, it is crucial to archive precipitation records from typical regions in CEC, for example, the Yangtze River Valley, to further confirm the tripolar precipitation pattern on orbital time scales.

On the modeling side, due to the model spread in simulating monsoonal precipitation in CEC, some uncertainties remain in the simulated tripolar precipitation pattern in monsoonal China on orbital timescales. This model spread can be observed in an earlier model-comparison for mid-Holocene simulations (Jiang, Tian, & Lang, 2013; Liu, Wen, et al., 2014), Holocene simulations (Sun et al., 2015) and also recent model-comparisons for last interglacial simulations (e.g., Leng et al., 2019; Nikolova et al., 2013; Scussolini et al., 2019; Sjolte & Hoffmann, 2014). For example, the CCSM3 (Nikolova et al., 2013) and the CESM (Leng et al., 2019) simulate decreased precipitation in CEC during the last interglacial, while LOVECLIM (Nikolova et al., 2013) and ECHAM4 (Sjolte & Hoffmann, 2014) do not. This model spread may come from possible ocean feedback (Liu, Harrison, et al., 2004) regulating the precipitation in monsoonal China. When the NH receives more insolation in summer, although all models show intensified subtropical highs (Jiang, Tian, & Lang, 2013), only those models that include stronger ocean feedbacks (Figure 8a) can produce the further northwestward extended west Pacific subtropical high, and thus can generate decreased precipitation in CEC (Liu, Harrison, et al., 2004).

Despite these uncertainties in proxies and simulations mentioned above, the tripole pattern in monsoonal China precipitation on orbital timescales is evident in our and early PMIP simulations, as well as some geological reconstructions (Figure 1; Figure 3). The key feature in the tripole precipitation pattern in

monsoonal China is the precipitation changes in CEC opposite to those in NC and SC. Compared to NC and SC, the precipitation in CEC is not only controlled by the intensity of EASM that brings moisture, but also influenced by the intensity of subtropical high pressures (Figures 8c and 8d). In the light of our simulations, on the orbital time scale, the NH summer insolation plays the pivotal role in affecting the coupled intensity of these two atmospheric circulation systems over East Asia, thus modulating the spatial precipitation variations in monsoonal China.

### 4.3. Complex Hydroclimatic Conditions in Monsoonal China

Our study well reconciles the conflicts between the widely believed concept in paleoclimate studies and the results in modern climate observations. Our simulations support the classic concept that stronger (weaker) interglacial (glacial) EASM brings more (less) precipitation to monsoonal China (e.g., Figure S2), and further show more temporal and spatial variability in precipitation in monsoonal China during the past glacial-interglacial cycles. Due to this variability, it remains possible that glacial precipitation was higher than modern. For example, in CEC, the annual precipitation is higher during MIS 4 than the PI. Glacial-interglacial hydroclimatic conditions might therefore be more complex than what we thought before. Such complex hydroclimatic conditions may be recorded by some indices, for example the snail fossil record, which is sensitive to the changes of temperature and precipitation (Wu et al., 2002). The stalagmites oxygen isotope records ( $\delta^{18}\text{O}$ ) in CEC likely reflect the variations in the intensity of EASM, as earlier studies (e.g., Liu, Wen, et al., 2014) and our results suggest. Most likely, the stalagmites  $\delta^{18}\text{O}$  record from CEC do not reflect variations in regional precipitation amount, since the precipitation in CEC shows a negative relationship to the EASM intensity and the stalagmites  $\delta^{18}\text{O}$  record from CEC. Therefore, it is necessary to obtain well-dated proxies for precipitation amount in or near CEC in the future.

In summary, our simulations and comparison to paleoclimate proxies suggest that the tripolar precipitation pattern in monsoonal China likely occur on orbital timescales, in addition to the suborbital and decadal timescales. During the past glacial-interglacial cycles, the boreal summer insolation is the primary forcing for the intensity of EASM. However, in addition to the intensity of EASM, the precipitation in CEC is further modulated by the intensity and position of the subtropical high pressures. During the period with increased (reduced) boreal summer insolation, the CEC receives relatively less (more) precipitation, while NC and SC receive relatively more (less) precipitation. This temporal and spatial variability in precipitation in monsoonal China highlight the complex hydroclimatic conditions in monsoonal China, and strongly calls for new explicit precipitation records with good age controls from the Yangtze River Valley.

### Data Availability Statement

The authors would like to thank three anonymous referees whose detailed comments helped us to greatly improve this manuscript. NorESM is available from <https://github.com/NorESMhub/NorESM/tree/1.0.0>. The paleoclimate data from monsoonal China were previously published in related references. The model results are available at <https://doi.org/10.5281/zenodo.4476384>.

### Acknowledgments

This study was jointly supported by the National Natural Science Foundation of China (Grant No. 41888101), by the National Key Research and Development Program of China (Grant No. 2018YFA0605602), the Norwegian Research Council (Project No. 221712, 229819, and 26261), and the Bjerknes Centre for Climate Research. All NorESM-L simulations are carried out on the cluster supported by the department of Atmospheric Science, China University of Geosciences, Wuhan.

### References

- Beck, J. W., Zhou, W., Li, C., Wu, Z., White, L., Xian, F., et al. (2018). A 550,000-year record of East Asian monsoon rainfall from  $^{10}\text{Be}$  in loess. *Science*, 360(6391), 877–881. <https://doi.org/10.1126/science.aam5825>
- Bentsen, M., Bethke, I., Debernard, J. B., Iversen, T., Kirkevåg, A., Seland, Ø., et al. (2013). The Norwegian Earth System Model, NorESM1-M - Part 1: Description and basic evaluation of the physical climate. *Geoscientific Model Development*, 6(3), 687–720. <https://doi.org/10.5194/gmd-6-687-2013>
- Berger, A., & Loutre, M. F. (1991). Insolation values for the climate of the last 10 million years. *Quaternary Science Reviews*, 10(4), 297–317. [https://doi.org/10.1016/0277-3791\(91\)90033-q](https://doi.org/10.1016/0277-3791(91)90033-q)
- Berger, A. L. (1978). Long-term variations of caloric insolation resulting from the Earth's orbital elements. *Quaternary Research*, 9(2), 139–167. [https://doi.org/10.1016/0033-5894\(78\)90064-9](https://doi.org/10.1016/0033-5894(78)90064-9)
- Chen, F., Xu, Q., Chen, J., Birks, H., Liu, J., Zhang, S., et al. (2015). East Asian summer monsoon precipitation variability since the last deglaciation. *Scientific Reports*, 5(1), 11186. <https://doi.org/10.1038/srep11186>
- Cheng, H., Edwards, R. L., Sinha, A., Spötl, C., Yi, L., Chen, S., et al. (2016). The Asian monsoon over the past 640,000 years and ice age terminations. *Nature*, 534(7609), 640–646. <https://doi.org/10.1038/nature18591>
- Cheng, H., Zhang, H., Zhao, J., Li, H., Ning, Y., & Kathayat, G. (2019). Chinese stalagmite paleoclimate researches: A review and perspective. *Science China Earth Sciences*, 62(10), 1489–1513. <https://doi.org/10.1007/s11430-019-9478-3>

- Ding, Y., Wang, Z., & Sun, Y. (2008). Inter-decadal variation of the summer precipitation in East China and its association with decreasing Asian summer monsoon. Part I: Observed evidences. *International Journal of Climatology*, 28(9), 1139–1161. <https://doi.org/10.1002/joc.1615>
- Eaton, B. (2010). *User's Guide to the Community Atmosphere Model CAM-CAM-5.1[J]*. Retrieved from NCAR. <https://www.cesm.ucar.edu/models/cesm1.0/cam>
- Huang, E., Chen, Y., Schefuß, E., Steinke, S., Liu, J., Tian, J., et al. (2018a). Precession and glacial-cycle controls of monsoon precipitation isotope changes over East Asia during the Pleistocene. *Earth and Planetary Science Letters*, 494, 1–11. <https://doi.org/10.1016/j.epsl.2018.04.046>
- Huang, X., Pancost, R. D., Xue, J., Gu, Y., Evershed, R. P., & Xie, S. (2018b). Response of carbon cycle to drier conditions in the mid-Holocene in central China. *Nature Communications*, 9(1), 1–9. <https://doi.org/10.1038/s41467-018-03804-w>
- Jia, G., Bai, Y., Yang, X., Xie, L., Wei, G., Ouyang, T., et al. (2015). Biogeochemical evidence of Holocene East Asian summer and winter monsoon variability from a tropical maar lake in southern China. *Quaternary Science Reviews*, 111, 51–61. <https://doi.org/10.1016/j.quascirev.2015.01.002>
- Jiang, D., Lang, X., Tian, Z., & Guo, D. (2011). Last glacial maximum climate over China from PMIP simulations. *Palaeogeography, Palaeoclimatology, Palaeoecology*, 309(3–4), 347–357. <https://doi.org/10.1016/j.palaeo.2011.07.003>
- Jiang, D., Tian, Z., & Lang, X. (2013). Mid-Holocene net precipitation changes over China: Model-data comparison. *Quaternary Science Reviews*, 82, 104–120. <https://doi.org/10.1016/j.quascirev.2013.10.017>
- Jiang, W., Guo, Z., Sun, X., Wu, H., Chu, G., Yuan, B., et al. (2006). Reconstruction of climate and vegetation changes of Lake Bayanchagan (Inner Mongolia): Holocene variability of the East Asian monsoon. *Quaternary Research*, 65(3), 411–420. <https://doi.org/10.1016/j.yqres.2005.10.007>
- Jin, L., Schneider, B., Park, W., Latif, M., Khon, V., & Zhang, X. (2014). The spatial-temporal patterns of Asian summer monsoon precipitation in response to Holocene insolation change: A model-data synthesis. *Quaternary Science Reviews*, 85, 47–62. <https://doi.org/10.1016/j.quascirev.2013.11.004>
- Kong, W., Swenson, L. M., & Chiang, J. C. H. (2017). Seasonal transitions and the westerly jet in the Holocene East Asian summer monsoon. *Journal of Climate*, 30(9), 3343–3365. <https://doi.org/10.1175/jcli-d-16-0087.1>
- Kuang, X., & Zhang, Y. (2006). Impact of the position abnormalities of East Asian subtropical westerly jet on summer precipitation in middle-lower reaches of Yangtze River (in Chinese with English abstract). *Plateau Meteorology*, 25(3), 382–389.
- Laskar, J., Robutel, P., Joutel, F., Gastineau, M., Correia, A. C. M., & Levrard, B. (2004). A long-term numerical solution for the insolation quantities of the Earth. *Astronomy & Astrophysics*, 428(1), 261–285. <https://doi.org/10.1051/0004-6361:20041335>
- Leng, S., Zhang, Z., & Dai, G. (2019). Two climate model simulation of MIS 5e climate in China (in Chinese with English abstract). *Quaternary Sciences*, 39(6), 1357–1371. <https://doi.org/10.11928/j.issn.1001-7410.2019.06.04>
- Li, T., Liu, F., Abels, H. A., You, C.-F., Zhang, Z., Chen, J., et al. (2017). Continued obliquity pacing of East Asian summer precipitation after the mid-Pleistocene transition. *Earth and Planetary Science Letters*, 457, 181–190. <https://doi.org/10.1016/j.epsl.2016.09.045>
- Lisiecki, L. E., & Raymo, M. E. (2005). A Pliocene-Pleistocene stack of 57 globally distributed benthic  $\delta^{18}\text{O}$  records. *Paleoceanography*, 20(1). <https://doi.org/10.1029/2004pa001071>
- Liu, H., Gu, Y., Huang, X., Yu, Z., Xie, S., & Cheng, S. (2019). A 13,000-year peatland palaeohydrological response to the ENSO-related Asian monsoon precipitation changes in the middle Yangtze Valley. *Quaternary Science Reviews*, 212, 80–91. <https://doi.org/10.1016/j.quascirev.2019.03.034>
- Liu, X., Battisti, D. S., & Donohoe, A. (2017). Tropical precipitation and cross-equatorial ocean heat transport during the mid-Holocene. *Journal of Climate*, 30(10), 3529–3547. <https://doi.org/10.1175/jcli-d-16-0502.1>
- Liu, Z., Harrison, S. P., Kutzbach, J., & Otto-Bliesner, B. (2004). Global monsoons in the mid-Holocene and oceanic feedback. *Climate Dynamics*, 22(2–3), 157–182. <https://doi.org/10.1007/s00382-003-0372-y>
- Liu, Z., Wen, X., Brady, E. C., Otto-Bliesner, B., Yu, G., Lu, H., et al. (2014). Chinese cave records and the East Asia Summer Monsoon. *Quaternary Science Reviews*, 83, 115–128. <https://doi.org/10.1016/j.quascirev.2013.10.021>
- Loulergue, L., Schilt, A., Spahni, R., Masson-Delmotte, V., Blunier, T., Lemieux, B., et al. (2008). Orbital and millennial-scale features of atmospheric  $\text{CH}_4$  over the past 800,000 years. *Nature*, 453(7193), 383–386. <https://doi.org/10.1038/nature06950>
- Lu, F., Ma, C., Zhu, C., Lu, H., Zhang, X., Huang, K., et al. (2019). Variability of East Asian summer monsoon precipitation during the Holocene and possible forcing mechanisms. *Climate Dynamics*, 52(1–2), 969–989. <https://doi.org/10.1007/s00382-018-4175-6>
- Lüthi, D., Le Floch, M., Bereiter, B., Blunier, T., Barnola, J.-M., Siegenthaler, U., et al. (2008). High-resolution carbon dioxide concentration record 650,000–800,000 years before present. *Nature*, 453(7193), 379–382. <https://doi.org/10.1038/nature06949>
- Miao, Y., Zhang, P., Lu, S., Wu, X., Li, L., Chen, H., et al. (2015). Late Quaternary pollen records from the Yangtze River Delta, East China, and its implications for the Asian monsoon evolution. *Arabian Journal of Geosciences*, 8(10), 7845–7854. <https://doi.org/10.1007/s12517-015-1777-8>
- Neale, R. B., Richter, J., Park, S., Lauritzen, P. H., Vavrus, S. J., Rasch, P. J., & Zhang, M. (2013). The Mean Climate of the Community Atmosphere Model (CAM4) in Forced SST and Fully Coupled Experiments. *Journal of Climate*, 26(14), 5150–5168. <https://doi.org/10.1175/jcli-d-12-00236.1>
- Nikolova, I., Yin, Q., Berger, A., Singh, U. K., & Karami, M. P. (2013). The last interglacial (Eemian) climate simulated by LOVECLIM and CCSM3. *Climate of the Past*, 9(4), 1789–1806. <https://doi.org/10.5194/cp-9-1789-2013>
- Ning, Y., Liu, W., & An, Z. (2008). A 130-ka reconstruction of precipitation on the Chinese Loess Plateau from organic carbon isotopes. *Palaeogeography, Palaeoclimatology, Palaeoecology*, 270(1–2), 59–63.
- Peltier, W. R., Argus, D. F., & Drummond, R. (2015). Space geodesy constrains ice age terminal deglaciation: The global ICE-6G\_C (VM5a) model. *Journal of Geophysical Research: Solid Earth*, 120(1), 450–487. <https://doi.org/10.1002/2014jb011176>
- Peterse, F., Martínez-García, A., Zhou, B., Beets, C. J., Prins, M. A., Zheng, H., & Eglinton, T. I. (2014). Molecular records of continental air temperature and monsoon precipitation variability in East Asia spanning the past 130,000 years. *Quaternary Science Reviews*, 83, 76–82. <https://doi.org/10.1016/j.quascirev.2013.11.001>
- Rodwell, M. J., & Hoskins, B. J. (2001). Subtropical anticyclones and summer monsoons. *Journal of Climate*, 14(15), 3192–3211. [https://doi.org/10.1175/1520-0442\(2001\)014<3192:saasm>2.0.co;2](https://doi.org/10.1175/1520-0442(2001)014<3192:saasm>2.0.co;2)
- Scussolini, P., Bakker, P., Guo, C., Stepanek, C., Zhang, Q., Braconnot, P., et al. (2019). Agreement between reconstructed and modeled boreal precipitation of the Last Interglacial. *Science Advances*, 5(11), eaax7047. <https://doi.org/10.1126/sciadv.aax7047>
- Shi, Z. G., Liu, X. D., Sun, Y. B., An, Z. S., Liu, Z., & Kutzbach, J. (2011). Distinct responses of East Asian summer and winter monsoons to astronomical forcing. *Climate of the Past*, 7(4), 1363–1370. <https://doi.org/10.5194/cp-7-1363-2011>



- Sjolte, J., & Hoffmann, G. (2014). Modelling stable water isotopes in monsoon precipitation during the previous interglacial. *Quaternary Science Reviews*, 85, 119–135. <https://doi.org/10.1016/j.quascirev.2013.12.006>
- Sun, Y., Kutzbach, J., An, Z., Clemens, S., Liu, Z., Liu, W., et al. (2015). Astronomical and glacial forcing of East Asian summer monsoon variability. *Quaternary Science Reviews*, 115, 132–142. <https://doi.org/10.1016/j.quascirev.2015.03.009>
- Thomas, E. K., Clemens, S. C., Prell, W. L., Herbert, T. D., Huang, Y., Liu, Z., et al. (2014). Temperature and leaf wax  $\delta^2\text{H}$  records demonstrate seasonal and regional controls on Asian monsoon proxies. *Geology*, 42(12), 1075–1078. <https://doi.org/10.1130/g36289.1>
- Thomas, E. K., Clemens, S. C., Sun, Y., Prell, W. L., Huang, Y., Gao, L., et al. (2016). Heterodynes dominate precipitation isotopes in the East Asian monsoon region, reflecting interaction of multiple climate factors. *Earth and Planetary Science Letters*, 455, 196–206. <https://doi.org/10.1016/j.epsl.2016.09.044>
- Wang, B., Wu, Z., Li, J., Liu, J., Chang, C.-P., Ding, Y., & Wu, G. (2008). How to measure the strength of the East Asian summer monsoon. *Journal of Climate*, 21(17), 4449–4463. <https://doi.org/10.1175/2008jcli2183.1>
- Wang, S., Lü, H., Liu, J., & Negendank, J. F. W. (2007). The early Holocene optimum inferred from a high-resolution pollen record of Huguangyan Maar Lake in southern China. *Chinese Science Bulletin*, 52(20), 2829–2836. <https://doi.org/10.1007/s11434-007-0419-2>
- Wang, Y., Wang, B., & Oh, J.-H. (2001). Impact of the Preceding El Niño on the East Asian Summer Atmosphere Circulation. *Journal of the Meteorological Society of Japan*, 79(1B), 575–588. <https://doi.org/10.2151/jmsj.79.575>
- Wang, Z., An, Z., Liu, Z., Qiang, X., Zhang, F., & Liu, W. (2018). Hydroclimatic variability in loess  $\delta\text{D}_{\text{wax}}$  records from the central Chinese Loess Plateau over the past 250 ka. *Journal of Asian Earth Sciences*, 155, 49–57. <https://doi.org/10.1016/j.jseas.2017.11.008>
- Wu, N., Liu, T., Liu, X., & Gu, Z. (2002). Mollusk record of millennial climate variability in the Loess Plateau during the Last Glacial Maximum. *Boreas*, 31(1), 20–27. <https://doi.org/10.1080/03009480210648>
- Xiao, J., Xu, Q., Nakamura, T., Yang, X., Liang, W., & Inouchi, Y. (2004). Holocene vegetation variation in the Daihai Lake region of north-central China: A direct indication of the Asian monsoon climatic history. *Quaternary Science Reviews*, 23(14–15), 1669–1679. <https://doi.org/10.1016/j.quascirev.2004.01.005>
- Xie, S., Evershed, R. P., Huang, X., Zhu, Z., Pancost, R. D., Meyers, P. A., et al. (2013). Concordant monsoon-driven postglacial hydrological changes in peat and stalagmite records and their impacts on prehistoric cultures in central China. *Geology*, 41(8), 827–830. <https://doi.org/10.1130/g34318.1>
- Yin, Q., & Berger, A. (2012). Individual contribution of insolation and  $\text{CO}_2$  to the interglacial climates of the past 800,000 years. *Climate Dynamics*, 38(3–4), 709–724. <https://doi.org/10.1007/s00382-011-1013-5>
- Zhang, H., Griffiths, M. L., Chiang, J. C. H., Kong, W., Wu, S., Atwood, A., et al. (2018). East Asian hydroclimate modulated by the position of the westerlies during Termination I. *Science*, 362(6414), 580–583. <https://doi.org/10.1126/science.aat9393>
- Zhang, R., Jiang, D., Zhang, Z., Cheng, Z., & Zhang, Q. (2017). Comparison of the climate effects of surface uplifts from the northern Tibetan Plateau, the Tianshan, and the Mongolian Plateau on the East Asian climate. *Journal of Geophysical Research: Atmospheres*, 122(15), 7949–7970. <https://doi.org/10.1002/2017jd026470>
- Zhang, Z., Ramstein, G., Schuster, M., Li, C., Contoux, C., & Yan, Q. (2014). Aridification of the Sahara desert caused by Tethys Sea shrinkage during the Late Miocene. *Nature*, 513(7518), 401–404. <https://doi.org/10.1038/nature13705>
- Zhang, Z., Yan, Q., Zhang, R., Colleoni, F., Ramstein, G., Dai, G., et al. (2020). Rapid waxing and waning of Beringian ice sheet reconcile climate records from around North Pacific. *Climate of the Past Discussions*.
- Zhang, Z. S., Nisancioglu, K., Bentsen, M., Tjiputra, J., Bethke, I., Yan, Q., et al. (2012). Pre-industrial and mid-Pliocene simulations with NorESM-L. *Geoscientific Model Development*, 5(2), 523–533. <https://doi.org/10.5194/gmd-5-523-2012>
- Zhou, T., & Yu, R. (2005). Atmospheric water vapor transport associated with typical anomalous summer rainfall patterns in China. *Journal of Geophysical Research*, 110(D8). <https://doi.org/10.1029/2004jd005413>
- Zhou, T., Yu, R., Zhang, J., Drange, H., Cassou, C., Deser, C., et al. (2009). Why the western Pacific subtropical high has extended westward since the late 1970s. *Journal of Climate*, 22(8), 2199–2215. <https://doi.org/10.1175/2008jcli2527.1>
- Zhou, W., Xian, F., Du, Y., Kong, X., & Wu, Z. (2014). The last 130 ka precipitation reconstruction from Chinese loess  $^{10}\text{Be}$ . *Journal of Geophysical Research: Solid Earth*, 119(1), 191–197. <https://doi.org/10.1002/2013jb010296>
- Zhou, W., Yu, X., Jull, A. J. T., Burr, G., Xiao, J. Y., Lu, X., & Xian, F. (2004). High-resolution evidence from southern China of an early Holocene optimum and a mid-Holocene dry event during the past 18,000 years. *Quaternary Research*, 62(1), 39–48. <https://doi.org/10.1016/j.yqres.2004.05.004>
- Zhu, J., & Wang, S. (2001). 80a-oscillation of summer rainfall over the east part of China and East-Asian Summer Monsoon. *Advances in Atmospheric Sciences*, 18(5), 1043–1051.
- Zhu, Z., Feinberg, J. M., Xie, S., Bourne, M. D., Huang, C., Hu, C., & Cheng, H. (2017). Holocene ENSO-related cyclic storms recorded by magnetic minerals in speleothems of central China. *Proceedings of the National Academy of Sciences of the United States of America*, 114(5), 852–857. <https://doi.org/10.1073/pnas.1610930114>